STM JOURNALS

Journal of
Polymer & Composites

ISSN: 2321-2810 (Online)
ISSN: 2321-8525 (Print)
Volume 14, Special Issue 1, 2026
DOI (Journal): 10.37591/JoPC

https://journals.stmjournals.com/jopc

Research JoPC

Role of Strontium in Structural and Dielectric characterstics of Barium Titanate

Shivani K. Kapoor[1,*], Ekta Jain[2], Shweta Thakur[3], Ritu Tiwari[4], Madhuri Singh[5], Anchit Modi[6], A. Mishra[7], N.K. Gaur[8]

Abstract

$Ba_{0.75}Sr_{0.25}TiO_3$ (BST) compound was synthesized through the conventional solid-state reaction methodology, aimed at investigating its structural, microstructural, and dielectric characteristics. The structural characterization was executed employing X-ray diffraction (XRD), and the resultant diffraction patterns were refined utilizing the Rietveld method, which substantiated the establishment of a single-phase perovskite configuration exhibiting tetragonal symmetry and belonging to the P4mm space group. The refined lattice parameters revealed subtle distortions correlating with the substitution of Sr at the A-site of the $BaTiO_3$ lattice. The tetragonality factor also exhibited slight variations, indicating the influence of Sr incorporation on the symmetry of the crystal structure.Using Scanning Electron Microscopy (SEM), we demonstrated the existence of well-defined grains noted for substantial grain development and a solid microstructure, which are both favorable for boosting dielectric and ferroelectric effectiveness. The substitution of Sr for Ba was observed to exert a profound impact on the electronic environment, consequently modifying the characteristics of the Ti–O bonds and altering the local polar distortions within the lattice framework. These alterations contributed to the stabilization of ferroelectric ordering and enhanced the dielectric response of the material.Dielectric measurements demonstrated an elevation in the dielectric constant concomitant with Sr doping, which can be ascribed to augmented polarizability and optimized grain connectivity. Furthermore, the analysis of ferroelectric hysteresis (P–E) loops revealed increased remnant polarization and coercive field, signifying improved ferroelectric behavior in comparison to undoped $BaTiO_3$. The introduction of Sr ions engenders local lattice strain and modulates the band structure, thereby playing a pivotal role in fine-tuning the electrical and ferroelectric properties of BST.In summary, the study elucidates that Sr doping in $BaTiO_3$ effectively modulates both the structural and dielectric attributes, rendering $Ba_{0.75}Sr_{0.25}TiO_3$ a compelling candidate for electronic and capacitor-based applications that necessitate materials with superior dielectric and ferroelectric performance.

***Author for Correspondence**
Shivani K. Kapoor

[1]Research Scholar, School of Physics, Devi Ahilya University, Indore, Madhya Pradesh, India
[2]Professor, Department of Applied Science, Sagar Institute of Research & Technology-Excellence, Bhopal, Madhya Pradesh, India
[3]Associate professor, Department of Basic Science, Oriental Institute of Science and Technology, Bhopal, Madhya Pradesh, India
[4]Professor, Department of Applied Science, Sagar Institute of Research and Technology, Bhopal, Madhya Pradesh, India
[5]Assistant Professor, Department of Applied Science, Sagar Institute of Research and Technology, Bhopal, Madhya Pradesh, India
[6]Professor, Department of Basics Sciences, IITM, IES University, Bhopal, Madhya Pradesh, India
[7]Professor, School of Physics, Devi Ahilya University, Indore, Madhya Pradesh, India
[8]Professor, Department of Physics, Barkatullah University, Bhopal, Madhya Pradesh, India

Received Date: June 10, 2025
Accepted Date: August 06, 2025
Published Date: February 10, 2026

Citation: Shivani K. Kapoor, Ekta Jain, Shweta Thakur, Ritu Tiwari, Madhuri Singh, Anchit Modi, A. Mishra, N.K. Gaur. Role of Strontium in Structural and Dielectric characterstics of Barium Titanate. Journal of Polymer & Composites. 2026; 14(Special Issue 1): S1157–S1163p.

Keywords: Perovskite structure, tetragonal symmetry, SEM, ferroelectric behavior, electrical measurements, P-E loop analysis

INTRODUCTION

Perovskite oxides belong to a wide-ranging category of functional materials noted for the general chemical formula ABO_3, wherein the A-site is primarily occupied by a larger alkali, alkaline-earth, or rare-earth cation, while a smaller transition

metal cation occupies the B-site [1]. These materials are recognized for their exceptional structural adaptability and compositional versatility, facilitating a broad spectrum of cation substitutions at both the A and B sites [2, 3]. In their most efficient crystalline arrangement, perovskites reveal a cubic structure featuring the A-site cation at the center of the cube, the B-site cation at the corners, and oxygen anions at the centers of the cube faces [4]. However, owing to disparities in ionic radii, charge distributions, and bonding characteristics, the majority of perovskites diverge from the ideal cubic symmetry and undergo structural distortions that result in lower-symmetry phases, including tetragonal, orthorhombic, or rhombohedral systems.

These structural distortions generally encompass the tilting and rotation of the BO_6 octahedra, the displacement of A- and B-site cations from their symmetrical positions, and the shifting of anions, all of which are instrumental in determining the functional properties of perovskite materials.

Such forms of structural irregularities might trigger the onset of ferroelectricity, antiferroelectricity, piezoelectricity, along with their corresponding phase transitions.The complex synergy between lattice distortions and electric dipole moments in perovskites contributes significantly to their remarkable allure for diverse technological applications, covering sensors, actuators, energy storage systems, and nonvolatile memory solutions.

Among the plethora of perovskite oxides examined thus far, barium titanate ($BaTiO_3$, BTO) is distinguished as a prototypical ferroelectric material that manifests a substantial spontaneous polarization attributable to the displacement of Ti^{4+} ions within the TiO_6 octahedral framework [5, 6]. This displacement-induced ferroelectric behavior is a consequence of the relative shift between the Ti and O atoms in relation to the Ba ion, culminating in a non-centrosymmetric structure below the Curie temperature. Accordingly, $BaTiO_3$ has been widely applied in capacitors, piezoelectric transducers, thermistors, and electro-optic modulators.

In recent years, significant efforts have been dedicated to augmenting the electrical performance and thermal stability of $BaTiO_3$ ceramics through cation doping methodologies. Both A-site and B-site doping techniques have been validated as effective in transforming the dielectric, ferroelectric, and structural aspects of BTO [7, 8]. These modifications stem from alterations in lattice strain, defect chemistry, polarization mechanisms, and electronic band structure. Notably, doping has emerged as a pivotal instrument for customizing the material's response to fulfill the rigorous requirements of commercial electronic components such as multilayer ceramic capacitors (MLCCs), microwave phase shifters, and tunable filters.

Despite its advantageous dielectric properties, pure $BaTiO_3$ is constrained by limitations such as a high temperature dependency of the dielectric constant and insufficient thermal stability, which impede its applicability in challenging environments [6–8]. To mitigate these deficiencies, a multitude of investigations have sought to explore the incorporation of dopants possessing varied ionic radii and valence states. Among these dopants, strontium (Sr^{2+}) has garnered significant interest as a potential A-site dopant due to its comparatively smaller ionic radius (1.44 Å) in relation to Ba^{2+} (1.61 Å), resulting in compressive lattice strain and enhanced structural coherence.

Strontium doping in $BaTiO_3$ has been demonstrated to significantly enhance crucial dielectric and ferroelectric characteristics, encompassing dielectric permittivity, breakdown strength, and thermal stability. Moreover, the substitution of Sr can facilitate the reduction of dielectric losses and the modulation of the Curie temperature, rendering Sr-doped $BaTiO_3$ (BST) particularly suitable for high-frequency applications and energy storage mechanisms [9]. The introduction of the Sr^{2+} ion at the Ba site alters the A-site environment and instigates nuanced modifications in the Ti–O–Ti bond angles, consequently influencing the overall polarizability and lattice dynamics of the material.

Nonetheless, prior studies have indicated that augmenting Sr concentration beyond specific thresholds may result in a decline in dielectric performance, especially within microwave devices, where a significant reduction in the dielectric constant is noted at elevated doping levels [10]. This finding accentuates the necessity of optimizing the Sr concentration to achieve an equilibrium between dielectric enhancement and structural integrity.

This research effort emphasizes the creation and evaluation of $Ba_{0.75}Sr_{0.25}TiO_3$ (BST) ceramics, in which 25 mol% of Ba^{2+} is exchanged for Sr^{2+}. This particular concentration was chosen based on previous research suggesting an optimal spectrum for attaining enhanced dielectric and ferroelectric attributes without incurring substantial structural degradation. The BST ceramics were synthesized employing the conventional solid-state reaction methodology, a cost-effective and scalable approach that is adept for yielding high-purity ceramic materials. A detailed characterization of the produced samples was executed employing X-ray diffraction (XRD) for phase analysis and Rietveld refinement, scanning electron microscopy (SEM) for microstructural evaluation, and dielectric and ferroelectric tests to analyze the electrical behavior.

This examination aims to reveal the consequences of 25% Sr doping on the structural symmetry, grain morphology, dielectric responses, and ferroelectric characteristics found in $BaTiO_3$ ceramics. The findings presented in this manuscript are intended to contribute to the ongoing endeavors aimed at optimizing perovskite-based dielectrics for implementation in advanced electronic devices and multifunctional systems.

EXPERIMENTAL DETAILS

The $Ba_{1-x}Sr_xTiO_3$ ($x = 0.25$) sample was synthesized through the high-temperature solid-state reaction techniques whose schematic diagram is shown in Figure 1. Stoichiometric amounts of the initial oxides, specifically $BaCO_3$, $SrCO_3$, and TiO_2 (Sigma Aldrich, 99.9% purity), were precisely measured. Subsequently, all chemical components were thoroughly ground and homogenized in an agate mortar with a pestle, utilizing acetone as the liquid medium. The first calcination of the mixed sample occurred at 800˚C for 12 hours. After regrinding the sample for 2 hours, the second calcination took place at 1000˚C for 12 hours. The resulting powder was then compacted into a pellet with a diameter of 10 mm and a thickness of approximately 1 to 3 mm using the hydraulic press, applying a pressure of around 8-10 tons. To achieve further densification, the resulting pellet underwent sintering at 1250˚C for 24 hours [11]. This multi-step synthesis and processing method ensures the formation of a well-prepared and dense $Ba_{1-x}Sr_xTiO_3$ ceramic sample.

To determine the purity and crystal structure of the sample, a powdered X-ray diffraction analysis was performed at ambient temperature using a D8 high-resolution X-ray diffractometer with CuKα ($\lambda = 1.5418$ Å) radiation. Lattice constants were determined using a conventional technique, displaying a robust correlation with PCPDF file no. (82-2234) in space group P4mm (99).

Figure 1. The schematic diagram of synthesis of $Ba_{0.75}Sr_{0.25}TiO_3$ Compound.

For electrical characterization, the sintered disc was polished and coated with a layer of high-purity ultrafine silver paste to ensure optimal conductivity. Following a 30-minute drying period at 473˚C, dielectric measurements were conducted at an ambient temperature (300 K) across a frequency spectrum ranging from 100 Hz to 323 MHz. The surface morphology of the $Ba_{0.75}Sr_{0.25}TiO_3$ compound was investigated using a JSM-5410 scanning electron microscopy (SEM). Finally, ferroelectric properties were studied at ambient temperature using a radiant-precision material analyzer.

RESULTS AND DISCUSSIONS

Figure 2 displays the X-ray diffraction (XRD) patterns of the $Ba_{0.75}Sr_{0.25}TiO_3$ compound, spanning a 2θ range of 20° to 70°. The presence of all observable peaks identifies the pure perovskite structure, highlighting the significant influence of Sr doping on the crystal and phase structures. The sharp and intense diffraction peaks confirm the well-crystallized structure of $Ba_{0.75}Sr_{0.25}TiO_3$. Notably, the tetragonal symmetry (P4mm) is evident in the split (200) peak at approximately 2θ ~ 45˚ for BST, aligning with the characteristic traits of tetragonal symmetry in $BaTiO_3$. To conduct a comprehensive structural examination, the XRD pattern of the reported sample was subjected to Rietveld analysis using the FullProf software, as illustrated in Figure 3. The lattice parameters and structural factors obtained from the refinement are detailed in Table 1.

The Rietveld analysis demonstrates that the BST sample adopts a tetragonal P4mm space group [11]. The average value of the crystallite size of BST was calculated from the significant diffraction peak denoting the Debye-Scherrer formula. The average crystallite size is estimated to be D = 38.697 nm [12].

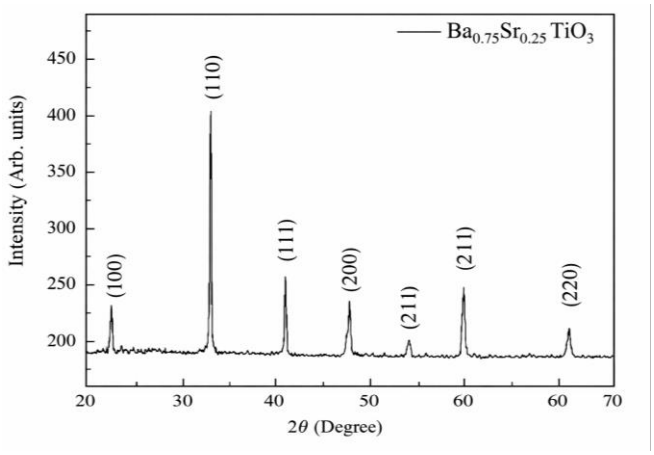

Figure 2. The XRD pattern of $Ba_{0.75}Sr_{0.25}TiO_3$ Compound.

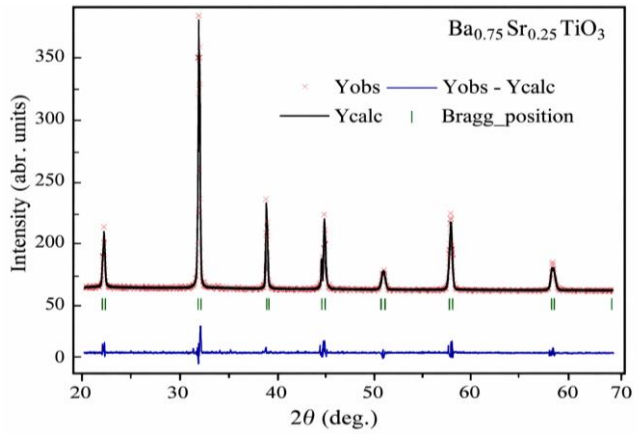

Figure 3. Rietveld refinement of $Ba_{0.75}Sr_{0.25}TiO_3$ compound.

Its grain size has a significant influence on the electrical characteristics of the bulk sample. To examine the morphology of the sintered pellets, a scanning electron microscope (SEM) analysis was conducted. Figure 4 displays the Scanning electron microscope image of the BST pellet. The average grain size was determined using the linear intercept method (not described here) in ImageJ software. The approximate grain size of the BST sample was found to be 1.009 μm.

The choice of material for specific device applications hinges on key parameters such as dielectric permittivity and dielectric loss. To conduct electrical measurements on the BST sample, pellets were meticulously prepared and sintered at 1250˚C. The variation in the dielectric constant of BST at room temperature (300 K) across different frequencies is illustrated in Figure 5. The graph unmistakably depicts a sharp decline in dielectric permittivity as the functional frequency increases, reaching saturation at higher frequencies. This behavior aligns with the Maxwell-Wagner type of interfacial polarization mechanism, consistent with Koop's phenomenological theory [13, 14].

The dielectric loss of BST, dependent on the frequency at ambient temperature (300 K), is illustrated in Figure 5. The graph indicates a consistent behavior of the loss tangent (tan δ) up to 10^4 Hz, beyond which a relaxation peak emerges. This distinctive relaxation peak is attributed to the synchronization between the applied frequency and the hopping frequency of charge carriers [15].

In Figure 6, the ferroelectric data (P–E loop) for the BST compound at ambient temperature (300 K), measured at 50 Hz, are presented. For the BST compound, the saturation polarization (P_s) value is 0.084 μC/cm², the remnant polarization value is 0.01969 μC/cm², and the coercive field is 0.07798 kV/cm.

However, there is a noticeable leakage in the P-E loop, which is caused by Sr doping and introduces defects, such as oxygen vacancies, that act as charge carriers in the P-E loops. The polarization of a ferroelectric material is related to the application of an electric field. The presence of defects introduced by Sr doping causes Sr-doped $BaTiO_3$ to exhibit a "leaky" behavior in the P-E loop. The introduction of oxygen vacancies by Sr doping may increase the density of mobile charge carriers, resulting in a decrease in material polarization as the electric field is increased [16, 17]. This behavior deviates from the conventional hysteresis loop, where polarization typically increases and then saturates as the electric field rises [18, 19]. Additionally,

Table 1. Structural and reliability parameters obtained from the refinement for $Ba_{0.75}Sr_{0.25}TiO_3$.

Lattice Parameters	**Atomic Positions of $Ba_{0.75}Sr_{0.25}TiO_3$**				
Crystal system: Tetragonal					
a= 4.0012 b= 4.0012 c= 4.0310 V=64.534	***Atoms***	***Wyckoff***	***x***	***y***	***z***
	Ba/Sr	1a	0	0	0.035
	TI	1b	0.5	0.5	0.527
	O1	1b	0.5	0.5	1.182
α=β=γ=90˚	O2	2c	0.5	0	0.531
Reliable Factor					
R_p= 19.0	R_{wp}= 24.3	R_{exp}= 13.4	R_{bragg}=9.74	R_f=6.10	χ^2=1.98

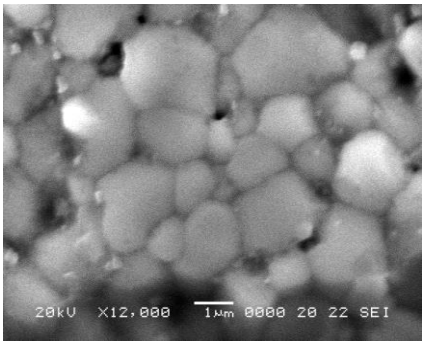

Figure 4. The scanning electron microscopy image of $Ba_{0.75}Sr_{0.25}TiO_3$ compound.

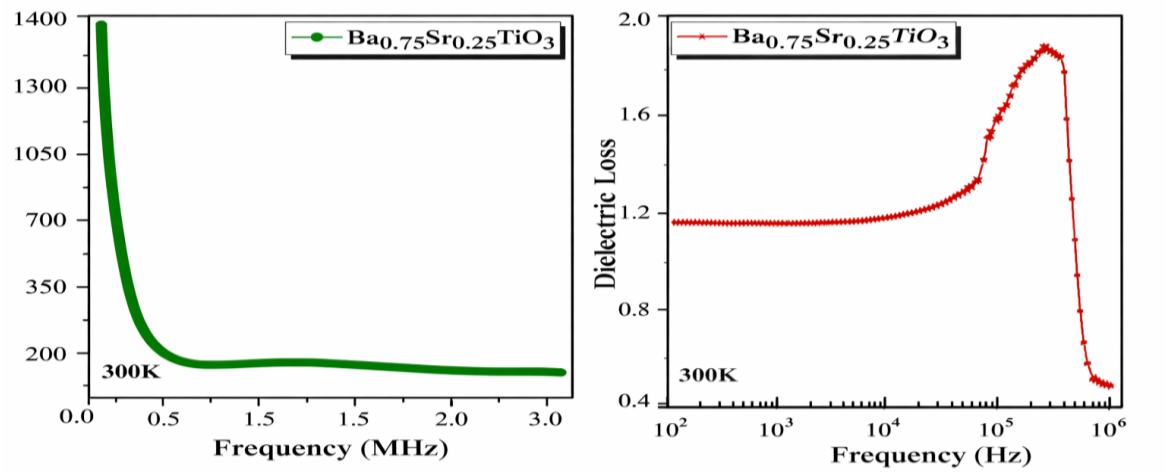

Figure 5. The left panel shows the dielectric constant and the right panel shows the dielectric loss of $Ba_{0.75}Sr_{0.25}TiO_3$ as a function of frequency.

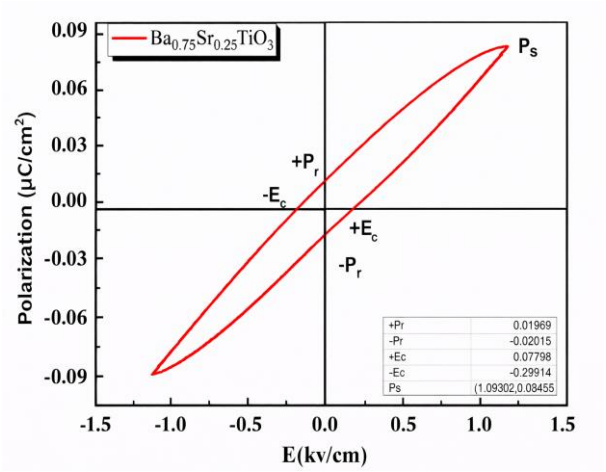

Figure 6. P-E hysteresis loop of $Ba_{0.75}Sr_{0.25}TiO_3$ measured at ambient temperature.

Sr doping may introduce irregularities into the crystal structure of $BaTiO_3$, leading to the formation of defect clusters and structural in-homogeneities. These in-homogeneities could create localized electric fields, prompting defects to move and causing the material to exhibit leakage.

CONCLUSION

The synthesis of $Ba_{0.75}Sr_{0.25}TiO_3$ was accomplished through the traditional solid-state synthesis method, and its structural, surface morphological, electrical, and ferroelectric properties were thoroughly examined. And the final value of refinement of raw XRD data comes out to be χ^2=1.98 which confirms the stability of the compound further the grain size value calculated via SEM image is 1.009 μm, and the value of saturation polarization (P_s) is 0.084 μC/cm². So, all functional properties were found to align with the structural attributes. Conclusively, XRD analysis revealed tetragonal properties, while SEM micrographs showcased a homogeneous surface morphology. The $Ba_{0.75}Sr_{0.25}TiO_3$ exhibited non-linear dielectric permittivity, a low dielectric loss tangent, and ferroelectric behavior. These distinctive characteristics have sparked significant interest in the investigation of Sr^{2+} doped $BaTiO_3$ recently. The observed properties make this material particularly valuable for the development of tunable microwave devices.

Declaration of Interest

The authors declare that there is no conflict of interest regarding the publication of this manuscript.

REFERENCES

1. Modi, D. K. Pandey, S. Bhattacharya, S. Mukherjee, G. S. Okram, N. K. Gaur, J. Mater. Sci: Mater. Electron 32 (2021) 23134–23145, https://doi.org/10.1007/s10854-021-06799-1.
2. Modi, M. Bhat, R. Parry, C. Chotia, P. Jain, G. S. Okram, N. K. Gaur, Emergent Mater. 5 (2022) 579–589, https://doi.org/10.1007/s42247-022-00357-z.
3. R. Yadav, A. Modi, K. Dubey, M. M. Malik, J. Mater. Sci: Mater. Electron 34 (2023) 1243, https://doi.org/10.1007/s10854-023-10630-4.
4. D. K. Pandey, A. Modi, N. K. Gaur, J. Supercond. Nov. Magn. 33 (2020) 1433–1438, https://doi.org/10.1007/s10948-019-05341-z.
5. T. Kim, H. Lim, Y. Lee, B. Kim, RSC Adv. 10 (2020) 29278, https://doi.org/10.1039/D0RA04196C.
6. J. Su, J. Zhang, J. Mater. Sci: Mater. Electron 30, (2019) 1957–1975, https://doi.org/10.1007/s10854-018-0494-y.
7. L. Gao, Y. Wu, R. Li, J. Hai, X. Yue, Z. Xie, J. Alloys Compd. 648 (2015) 017–1023, https://doi.org/10.1016/j.jallcom.2015.06.267.
8. H. Jiao, K. Zhao, T. Bian, Y. Tang, J. Alloys Compd. 715 (2017) 73–82, https://doi.org/10.1016/j.jallcom.2017.04.299.
9. S. Sasikumar, R. Saravanan, S. Saravanakumar, J. Mater. Sci: Mater. Electron 29 (2018) 1198–1208, https://doi.org/10.1007/s10854-017-8022-z.
10. Y. Wang, Z. Shen, Y. Li, Z. Wang, W. Luo, Y. Hong, Ceram. Int. 41 (2015) 8252–8256, https://doi.org/10.1016/j.ceramint.2015.02.156.
11. D. K. Pandey, A. Modi, N. K. Gaur, DAE-SSPS 2018, AIP Conf. Proc. 2115 (2019) 030388; 2018 Dec 18–22 Hisar, Haryana, India;https://doi.org/10.1063/1.5113227.
12. K. Dubey, S. Dubey, V. Sahu, R. A. Parry, A. Modi, N. K. Gaur, Appl. Phys. A 128 (2022) 560, https://doi.org/10.1007/s00339-022-05681-z.
13. S.W. Kim, H. I. Choi, M. H. Lee, J. S. Park, D. J. Kim, D. Do, M. H. Kim, T. K. Song, W. J. Kim, Ceram. Int. 39 (2013) S487–S490, https://doi.org/10.1016/j.ceramint.2012.10.119.
14. T. Prodromakis, C. Papavassiliou, Appl. Surf. Sci. 255 (2009) 6989–6994, https://doi.org/10.1016/j.apsusc.2009.03.030.
15. P. Gupta, P. K. Mahapatra, R. N. P. Choudhary, Ceram. Int. 45 (2019) 22862–22871, https://doi.org/10.1016/j.ceramint.2019.07.329.
16. A.Kaur, L. Singh, K. Asokan, Ceram. Int. 44 (2018) 3751–3759, https://doi.org/10.1016/j.ceramint.2017.11.158.
17. P. Joshi, A. Modi, S. K. Kapoor, S. Tiwari, J. Shukla, A. Mishra, J. Mater. Sci: Mater. Electron 34 (2023) 1783, https://doi.org/10.1007/s10854-023-11202-2.
18. S. Dubey, K. Dubey, V. Sahu, A. Modi, G. Pagare, F. Z. Haque, N. K. Gaur, J. Mater. Sci: Mater. Electron 34 (2023) 2312, https://doi.org/10.1007/s10854-023-11769-w.
19. A.Modi, M. A. Bhat, D. K. Pandey, N. K. Gaur, Mater. Lett 276 (2020) 128212, https://doi.org/10.1016/j.matlet.2020.128212

